Electronic Supporting Information (16 pages)

Three Redox States of a Diradical Acceptor-Donor-Acceptor Triad: Gating the Magnetic Coupling and the Electron Delocalization

Manuel Souto, [†] *Vega Lloveras,* [†] *Sergi Vela,* [‡] *Maria Fumanal,* [‡] *Imma Ratera,* [†,*] *and Jaume Veciana*[†,*]

[†] Institut de Ciència de Materials de Barcelona (ICMAB-CSIC)/CIBER-BBN, Campus Universitari de la UAB, 08193 Cerdanyola del Vallès (Barcelona), Spain

[‡] Laboratoire de Chimie Quantique, Université de Strasbourg, 4 rue Blaise Pascal, F-67000 Strasbourg, France

*E-mail: vecianaj@icmab.es, iratera@icmab.es

Table of Content

General methods for synthesis and characterization

All reagents and solvents employed for the syntheses were of high purity grade and were purchased from Sigma-Aldrich Co., Merck, and SDS. ^{1}H NMR spectra were recorded using a Bruker Avance 250, 400, 500 instruments and Me_4Si as an internal standard. Infrared spectra were recorded with Spectrum One FT-IR Spectroscopy instrument and UV/Vis/NIR spectra were measured using Cary 5000E Varian. ESR spectra were performed with a Bruker ESP 300 E equipped with a rectangular cavity T102 that works with an X-band (9.5 GHz). The solutions were degassed by argon bubbling before the measurements. LDI/TOF MS were recorded in a Bruker Ultraflex LDI-TOF spectrometer. Cyclic voltammetry measurements were obtained with a potentiostat 263a from EG&G Princeton Applied Research in a standard 3 electrodes cell. Dry solvents were used in the chemical reactions and in the cyclic voltammetries. The solvents used for optical spectroscopy and ESR measurements were of HPLC grade (ROMIL-SpS). In addition, for cyclic voltammetry experiments, CH_2Cl_2 was filtered over basic alumina to eliminate the acidic residues.

Synthesis of 2:

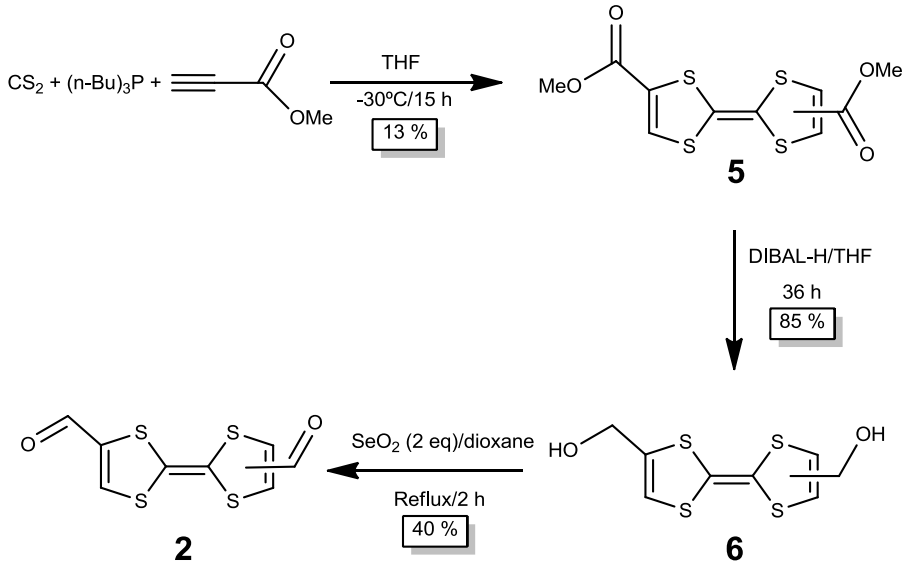

Scheme S1. Synthesis of the diformyl-TTF derivative **2**.

Compound 5: Tributylphosphine (20.3 g, 0.1 mol) was added dropwise to a solution of 10 ml of carbon disulfide in 50 ml of tetrahydrofuran at -10ºC under inert conditions and the deep maroon solution was stirred at room temperature for 1 hour. Next the mixture was cooled to -40ºC and a solution of methyl propiolate (8.4 g, 0.1 mol) in 20 ml of tetrahydrofuran was added dropwise. The temperature was maintained between -30ºC and -50ºC during the addition. The solution was warmed to room temperature and stirred overnight. Finally solvents were evaporated under reduced pressure, the residue was stirred with ether to crash out the product that and was filtered and washed with Et_2O. Then the product was purified by column chromatography using CH_2Cl_2 as eluent to give 4.2 g (13 %) of the red microcrystalline powder **5**. Characterization: ^{1}H-NMR (250 MHz, $CDCl_3$, δ(ppm): 7.35 (d, 2H, CH, J = 7.34 Hz); 3.82 (s, 6H, CH_3). FT-IR (ν cm^{-1}): 2956 (w); 2922 (w); 2852 (w); 1712 (s, C=O); 1548 (s); 1434 (m); 1244 (s); 1199 (m); 1045 (m); 940 (m); 829 (m); 820 (m); 763 (m); 725 (m). LDI-TOF (positive mode): *m/z* (amu/e^-): 320.377 ($M^{+\cdot}$).

Compound 6: 30 ml of DIBAL-H (1 M in THF) was added dropwise to a solution of **5** (1 g, 3.12 mmol) in 60 ml of tetrahydrofuran cooled at -70ºC under strict inert conditions. The color of the solution changes from red to yellow during the first hour of reaction. Then the solution was allowed to warm to room temperature and stirred overnight. The absence of TTF diester was confirmed by TLC and the reaction was hydrolyzed by the carefully addition of 10 ml of MeOH/HCl 12 M (3:1) mixture to the solution previously cooled with an ice bath. Then ether was

added to the mixture and the organic phase was washed with three portions of water (100 ml), dried with anhydrous $MgSO_4$ and solvents were evaporated under reduced pressure. Finally the product was purified by column chromatography of silica gel using a mixture of ether and hexane to obtain 738 mg (85 %) of TTF diol **6** as a light brown solid. Characterization: ^{1}H-NMR (250 MHz, DMSO-D_6, δ(ppm): 6.52 (s, 2H); 5.48 (t, 2H, *J* = 5.9 Hz); 4.20 (d, 4H, *J* = 5.84 Hz, CH_2OH). FT-IR (ν cm^{-1}): 3338 (s, OH); 3256 (s, OH); 2947 (m); 2918 (m); 2858 (m); 1587 (w); 1459 (m); 1443 (m); 1430 (m); 1369 (m); 1228 (m); 1092 (s); 1012 (s); 969 (m); 839 (w); 773 (w); 741 (w) 709 (w). LDI-TOF (positive mode): *m/z* (amu/e$^-$): 263.926 ($M^{+\cdot}$).

Compound 2: A solution of **6** (750 mg, 2.84 mmol) and 2 equivalents of selenium dioxide (630 mg)was heated under reflux for 2 h in dry dioxane (70 mL); the solution turned from yellow to dark red. Cooling of the solution resulted in the formation of a black precipitate of elemental selenium, which was filtered and washed thoroughly with dichloromethane. The solvent mixture was then evaporated under reduced pressure to produce a dark red oil, which was purified by SiO_2 column chromatography (eluent: hexane: Et_2O) to obtain **2** (295 mg, 40%) as a brownish powder. Characterization: ^{1}H-NMR (250 MHz, DMSO-D_6, δ(ppm): 9.54 (s, 2H, CHO); 8.27 and 8.28 (s, 2H). LDI-TOF (positive mode): *m/z* (amu/e$^-$): 259.729($M^{+\cdot}$).

Synthesis of diradical 1$^{\cdot\cdot}$:

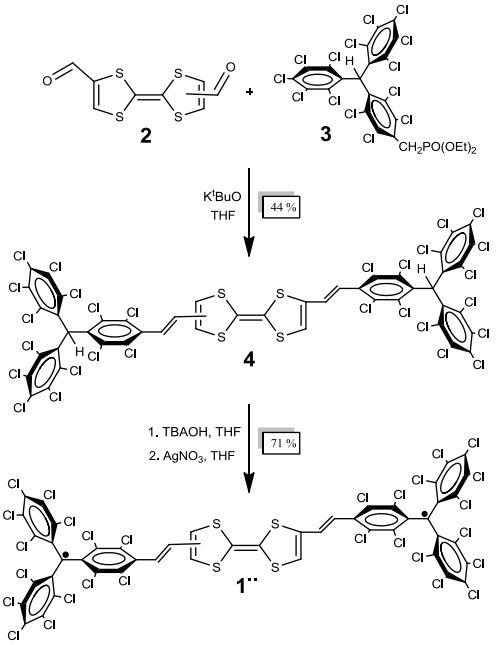

Scheme S2. Final synthetic steps of diradical **1**$^{\cdot\cdot}$. TBAOH = Tetrabutylammonium hydroxide.

Compound 4: 585 mg (0.67 mmol) of the phosphonated PTM derivative **3** were dissolved in 60 ml of anhydrous THF under strict inert conditions. The solution was cooled down to -78 ºC. Next, 150 mg (1.33 mmol) of potassium *tert*-butoxide were added and stirred for 20 minutes to form the yellow-orange ylide. Then 101 mg (0.39 mmol) of **2** were added and the reaction was warmed up to room temperature and stirred for 3 days. Then the mixture was washed with water, dried with anhydrous $MgSO_4$ and solvents were evaporated under reduced pressure. Finally the product was purified by column chromatography of silica gel using a mixture of ether and hexane to obtain to obtain 250 mg (44 %) of **4** (*E*+*Z*) as a red powder. Characterization: ^{1}H-NMR (250 MHz, C_6D_6, δ(ppm): 7.22 (s, 1H, αH); 7.21 (s, 1H, αH); 6,32 (dd, *J* = 16.0, 2.5 Hz, 2H, CH=CH); 6.18 (dd, *J* = 16.1, 6.2 Hz, 2H CH=CH); 5.53 (s, 2H, TTF). FT-IR (ν cm^{-1}): 2956 (w); 2922 (w); 2855 (w); 1614 (m, CH=CH); 1528 (m); 1455 (m); 1369 (m); 1336 (s); 1296 (s); 1276 (w); 1238 (w); 1206 (w); 1137 (m); 944 (m); 863 (w); 826 (w); 808 (s); 778 (m) 751 (m); 719 (w); 693 (m). LDI-TOF (positive mode): *m/z* (amu/e$^-$): 1704.559 ($M^{+\cdot}$); (negative mode): 1704.147 ($M^{-\cdot}$). Cyclic voltammetry (Bu_4NPF_6 0.15 M in CH_2Cl_2 as electrolyte): $E_{½}{}^1$=0.621 V; $E_{½}{}^2$=1.103 V.

Diradical 1$^{\cdot\cdot}$: 70 mg (0.04 mmol) of **4** were dissolved in 20 ml of distilled THF and 100 μl (0.10 mmol) of TBAOH 1.0 M in MeOH were added and stirred for 3 h under Ar atmosphere. Then 20 mg (0.12 mmol) of $AgNO_3$ were added and immediately stirred for 10 minutes. The solution was concentrated and the product was purified by flash column chromatography of silica gel using hexane as eluent to produce 50 mg (71 %) of a brownish powder. Characterization: FT-IR (ν cm^{-1}): 2952 (w); 2922 (w); 2855 (w); 1603 (m, CH=CH); 1504 (m); 1460 (m); 1376 (w); 1355 (2); 1335 (s); 1320 (s); 1278 (m); 1259 (s); 1162 (m); 1138 (w); 1118 (w); 935 (s); 866 (w); 817 (m); 777 (m) 752 (m); 735 (m); 711 (m). UV-VIS-NIR (CH_2Cl_2, λ_{max} in nm, ε in $M^{-1}\cdot cm^{-1}$): 299 (30752); 325 (27461); 387 (26506); 426 (16192); 522 (6303); 938 (1087). LDI-TOF (positive mode): *m/z* (amu/e^-): 1700.947 $[M]^{+\cdot}$; 1630.060 $[M\text{-}70]^+$; (negative mode): 1704.913 $[M]^{-\cdot}$; 1632.412 $[M\text{-}70]^+$. Cyclic voltammetry (Bu_4NPF_6 0.15 M in CH_2Cl_2 as electrolyte): $E_{½}^1$= -0.213 V; $E_{½}^2$= 0.591 V; $E_{½}^3$ =1.064 V. ESR (Toluene:CH_2Cl_2): g = 2.0027; a_1(H)=0.8 G (Half field at 1675 G).

^{1}H-NMR of 4

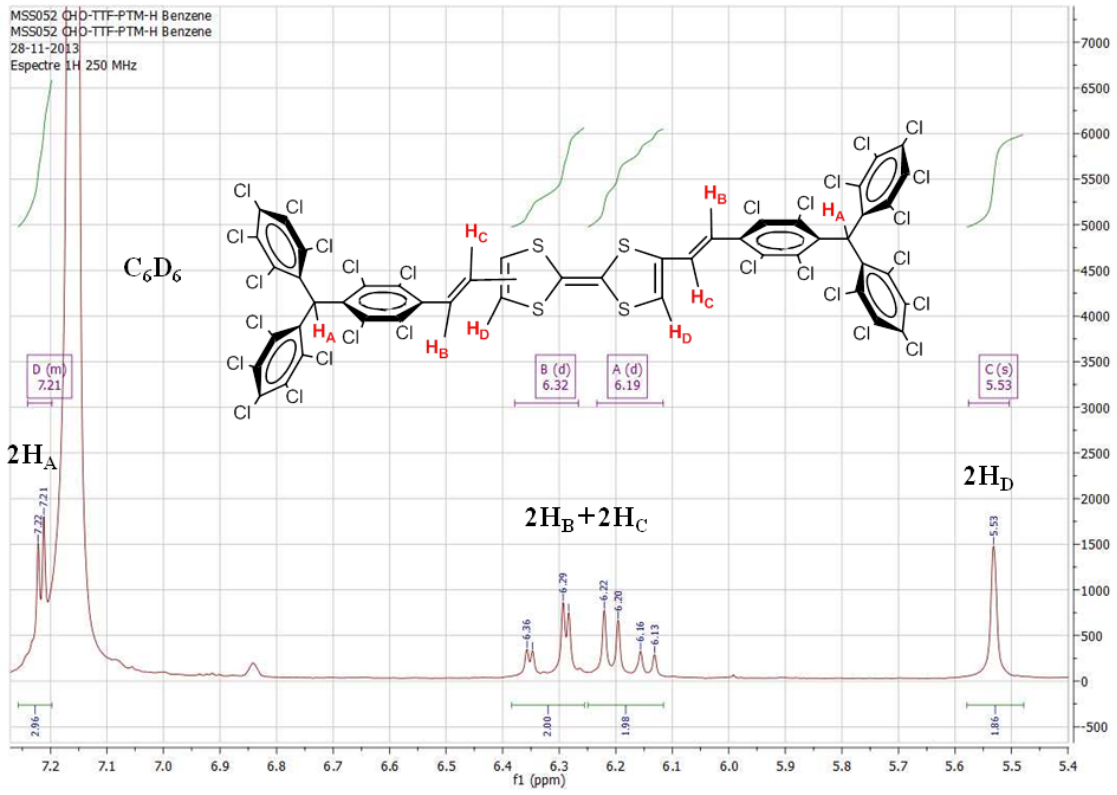

Figure S1. ^{1}H-NMR spectrum of compound **4** in C_6D_6 and protons observed in the ^{1}H-NMR spectrum.

Cyclic Voltammetry of 4

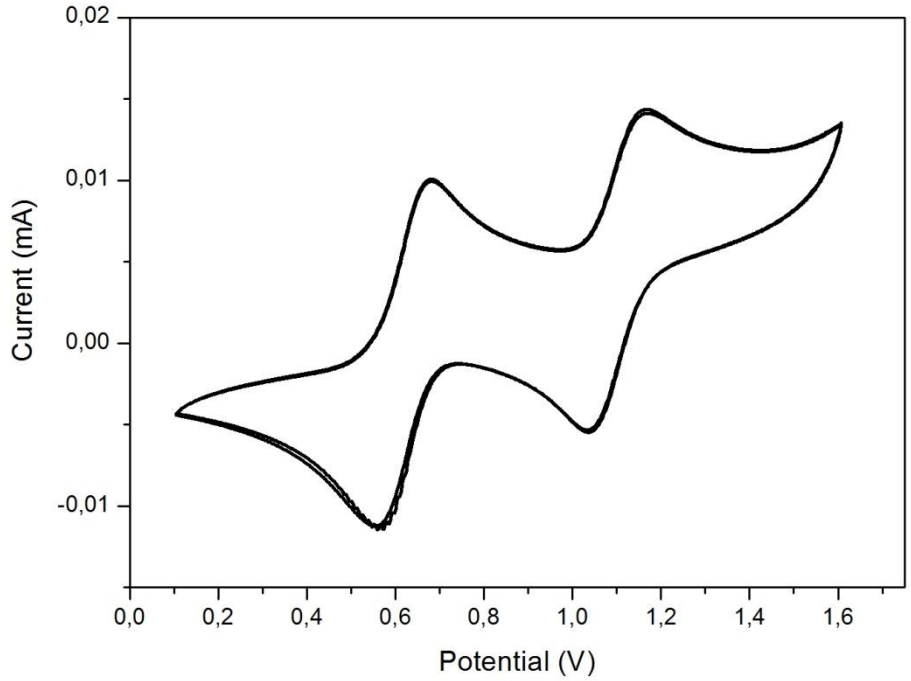

Figure S2. Cyclic voltammetry of solution of compound **4** in CH_2Cl_2 vs. Ag/AgCl using *n*-Bu_4PF_6 (0.1 M) as electrolyte at 300 K under argon at a scan rate of 0.1 V/s.

UV-vis spectrum of 4

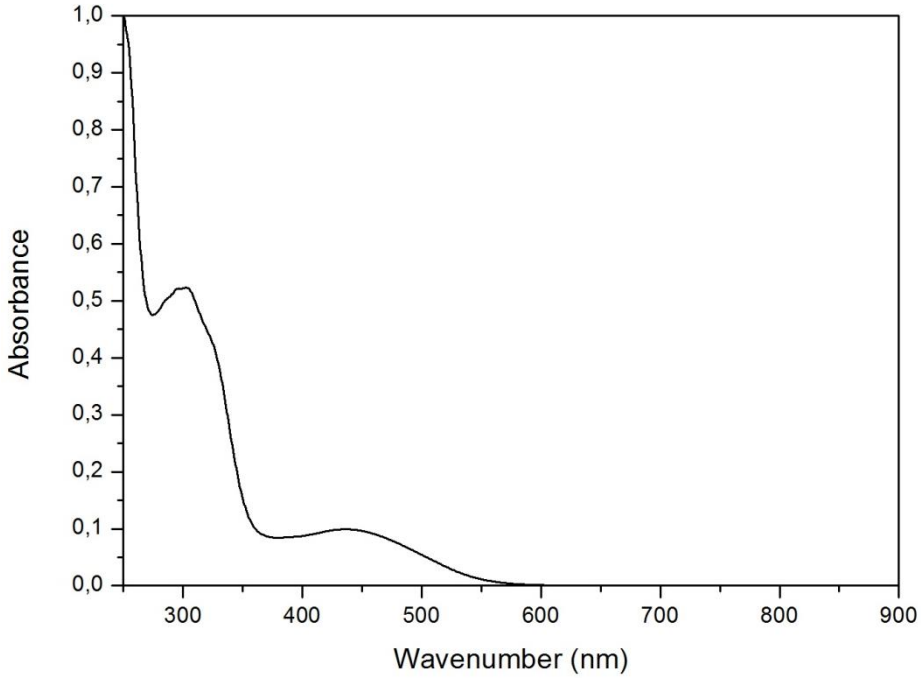

Figure S3. UV-Vis spectrum of a solution 0.05 mM of compound **4** in CH_2Cl_2 (black line).

IR spectra of 4 and 1¨

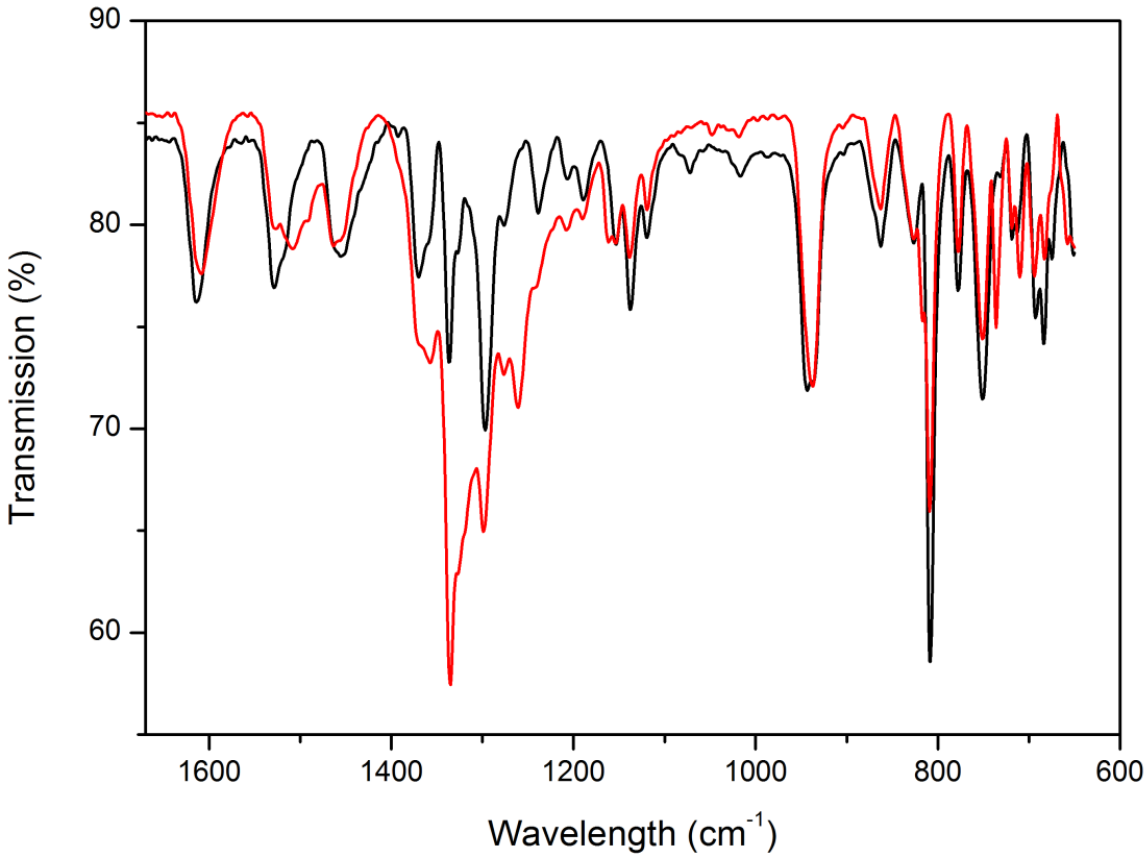

Figure S4. FT-IR spectra of compounds **4** (black line) and diradical **1**¨ (red line).

MALDI-TOF spectrum of 1··

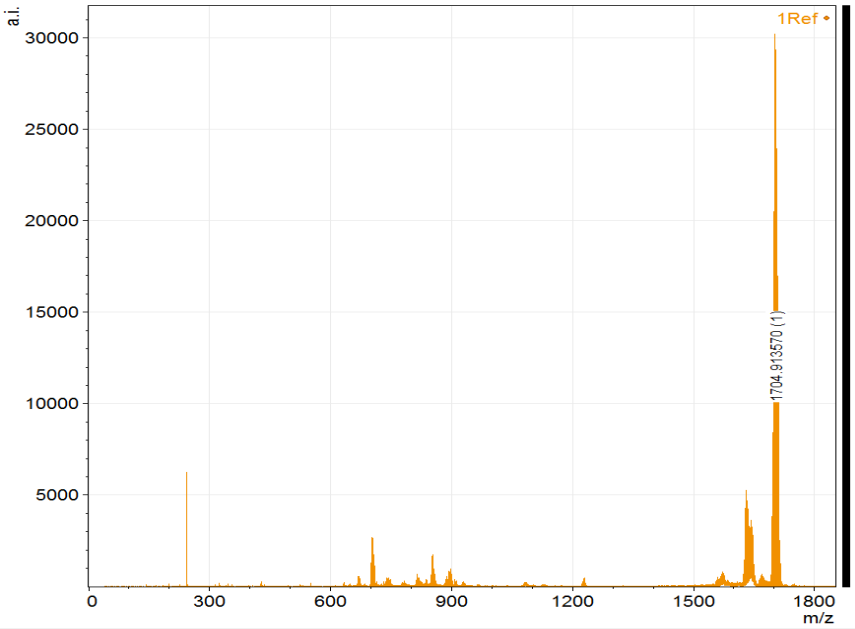

Figure S5. MALDI-TOF spectrum of diradical **1**¨ (negative mode) indicating the molecular mass of the compound.

Electrospray ionization for mass spectrometry (ESI-MS)

Instrument: LC/MSD-TOF (2006) (Agilent Technologies)
Intrumental conditions:

Capillary: 3.5 KV (negative)
Fragmentor: 225 V
Gas temperature: 325ºC
Nebulizing Gas: N_2 Pressure = 15 psi
Drying Gas: N_2 Glow = 7.0 l /min

Sample introduction. Samples (microliters) are introduced into the source with an HPLC system (Agilent 1100), using a mixtue of H_2O:CH_3CN 1:1 as eluent (100 ml/min),

ESI-MS spectrum of compound 4

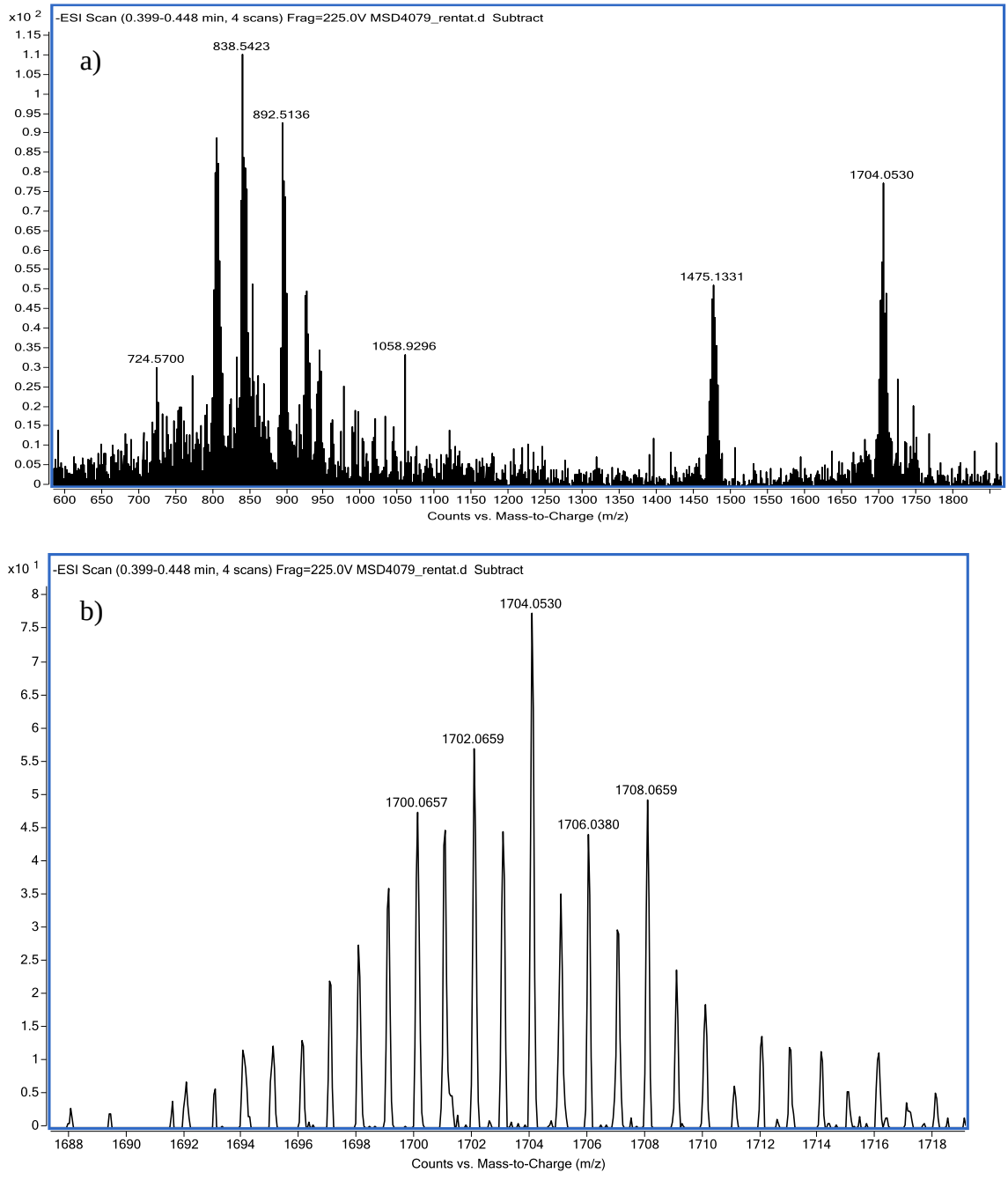

Figure S6. a) ESI-MS spectrum of compound **4** (mz/1705.06) and b) mass isotopic distribution of **4** (negative mode).

ESI-MS spectrum of compound 1··

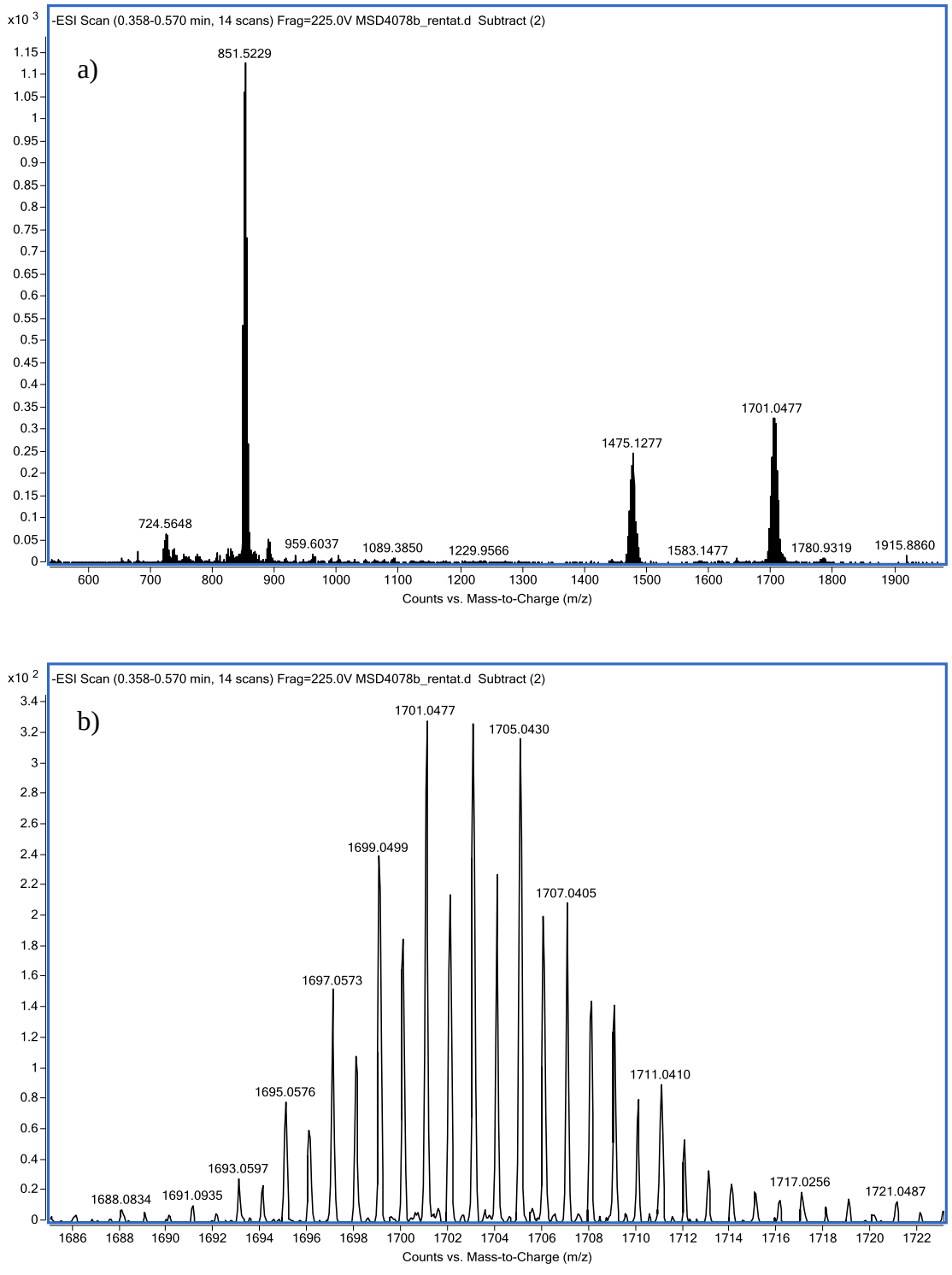

Figure S7. a) ESI-MS spectrum of compound **1··** (mz/1703.04) and b) mass isotopic distribution of **1··** (negative mode).

Chemical reduction of $\mathbf{1}^{\cdot\cdot}$

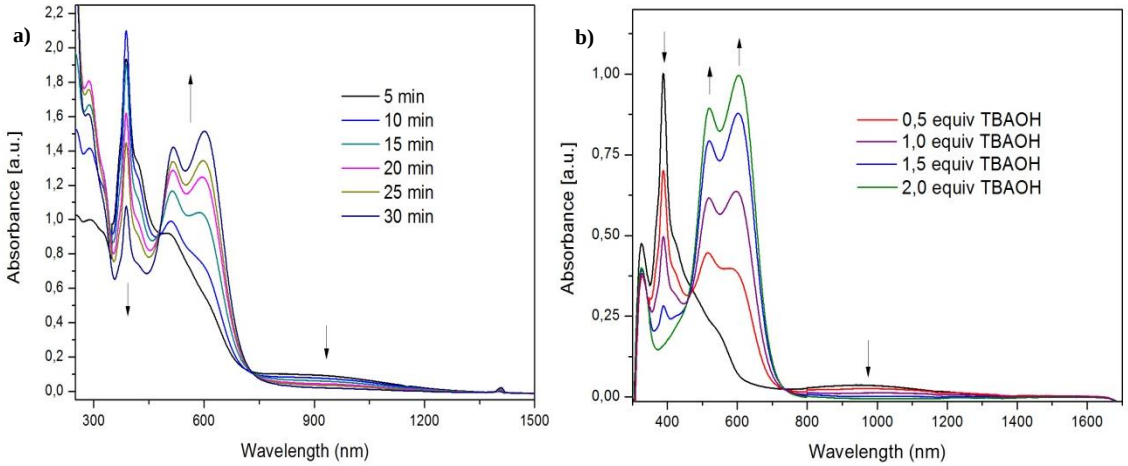

Figure S8. (*a*) Evolution of the UV-vis-NIR during the course of the formation of radical anion mixed-valence $\mathbf{1}^{\cdot-}$ in CH_2Cl_2 with metallic Cu. **(b)** Evolution of the UV-vis-NIR spectra during the course of the reduction of diradical $\mathbf{1}^{\cdot\cdot}$ to the formation of the radical anion $\mathbf{1}^{\cdot-}$ (1 equiv.) followed by the dianaion $\mathbf{1}^{2-}$ (2 equiv.) in THF arising from the subsequent addition of equivalent amounts of tetrabutylammonium hydroxide (TBAOH) until the formation of dianion.

Chemical oxidation of $\mathbf{1}^{\cdot\cdot}$

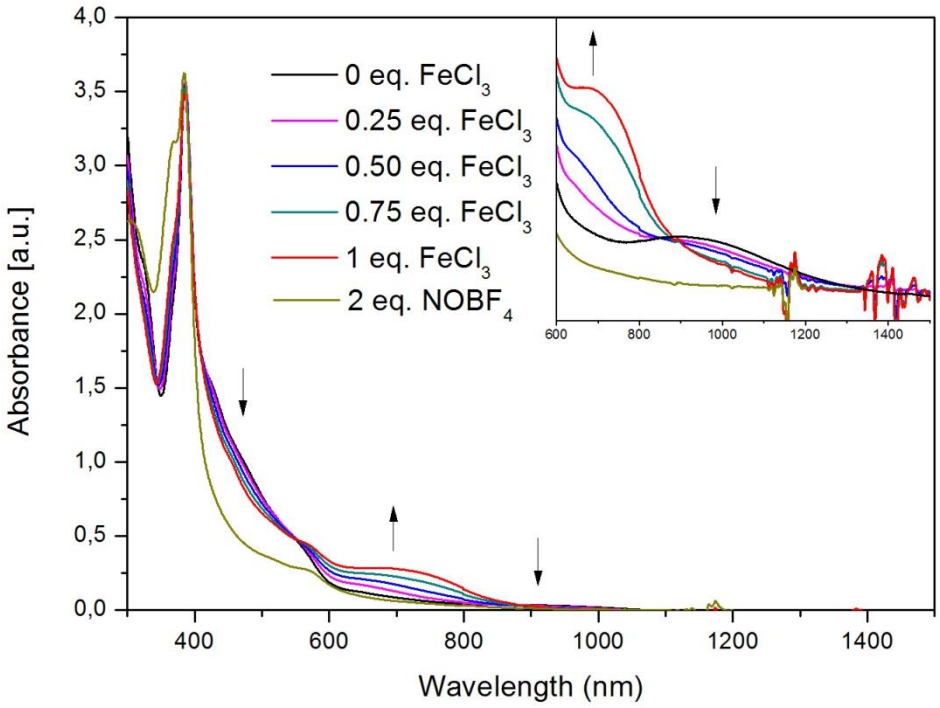

Figure S9. Evolution of the UV-vis-NIR spectra during the course of the oxidation of diradical $\mathbf{1}^{\cdot\cdot}$ in CH_2Cl_2 arising from the subsequent addition of equivalent amounts of $FeCl_3$ until the formation of $\mathbf{1}^{\cdot\cdot\cdot+}$ (red line) and further oxidation using nitrosium tetrafluoroborate to form $\mathbf{1}^{++}$ (brown line).

ESR of 1$^{\cdot\cdot}$

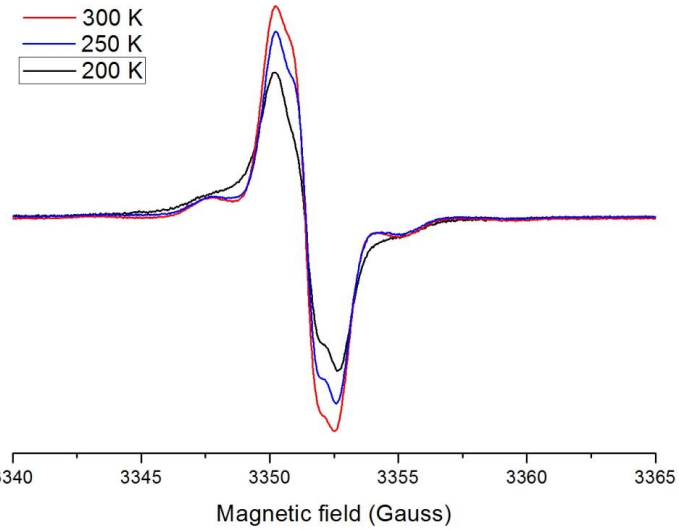

Figure S10. ESR spectra of 0.05 mM solution of diradical **1**$^{\cdot\cdot}$ in CH_2Cl_2 at 300 (red line), 250 (blue line) and 200 K (black line).

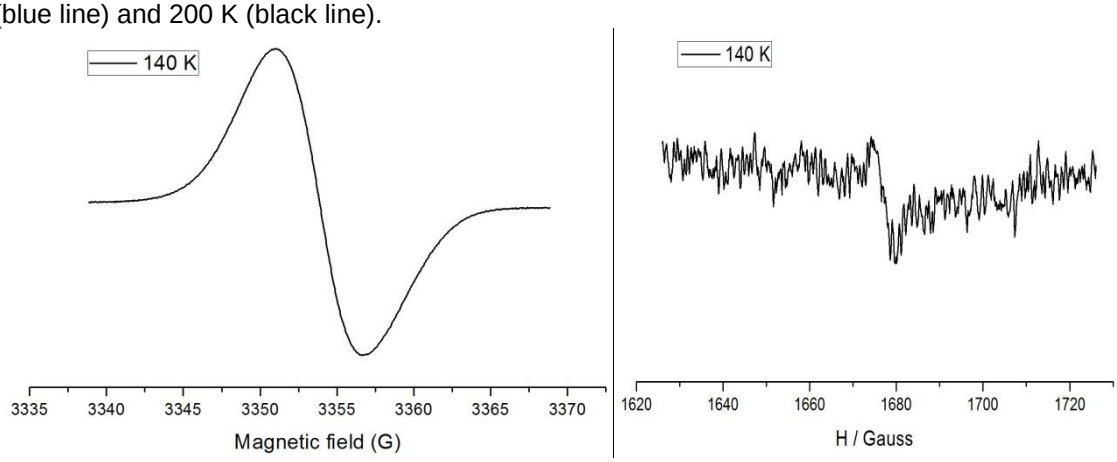

Figure S11. a) ESR spectra of 1 mM solution of diradical **1**$^{\cdot\cdot}$ in CH_2Cl_2 at 140 K. b) ESR spectra of 1 mM solution of diradical **1** in CH_2Cl_2 at 140 K at the half-field region.

ESR of radical-anion 1$^{\cdot-}$

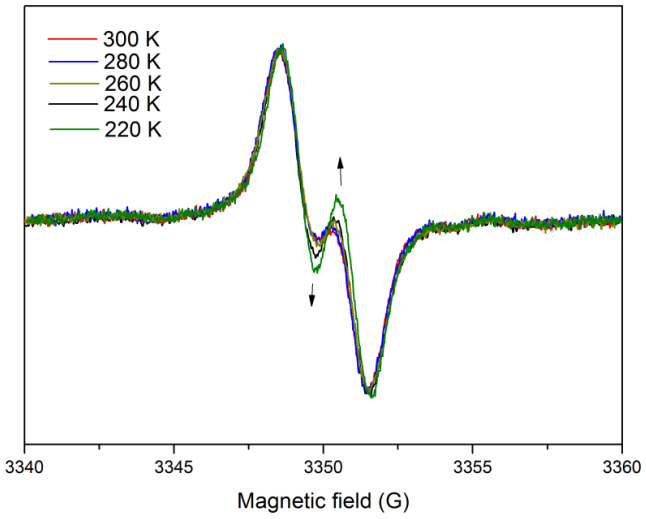

Figure S12. ESR spectra of 0.05 mM solution of mixed-valence **1**$^{\cdot-}$ in toluene/CH_2Cl_2 at 300 (red line), 280 (blue line), 260 (brown line), 240 (black line) and 220 K (green line).

ESR of triradical cation $\mathbf{1}^{\bullet\bullet\bullet+}$

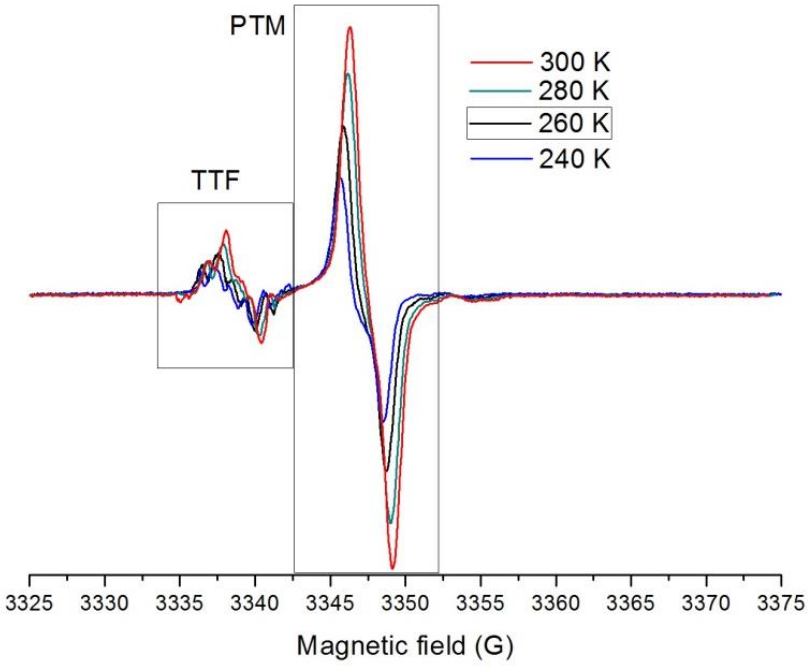

Figure S13. ESR spectra of 0.05 mM solution of triradical cation $\mathbf{1}^{\bullet\bullet\bullet+}$ in CH_2Cl_2 at 300 (red line), 280 (green line), 260 (black line) and 240 (blue line).

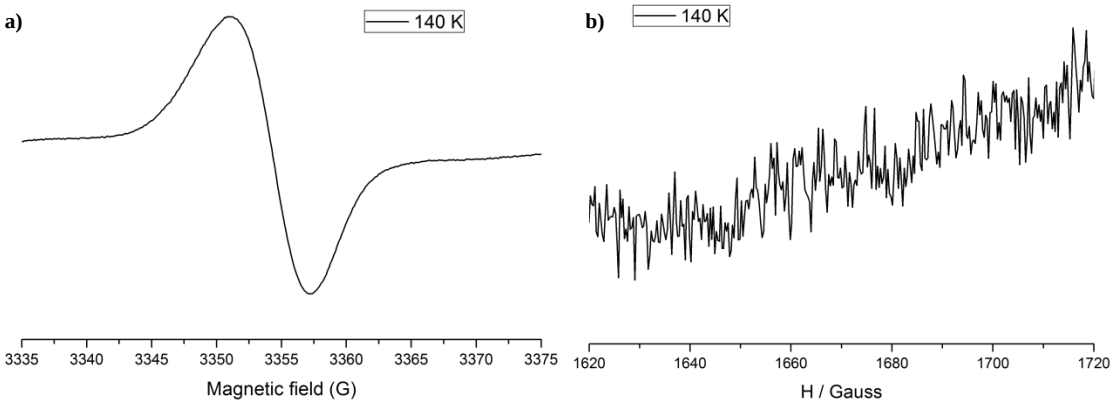

Figure S14. a) ESR spectra of 1 mM solution of triradical cation $\mathbf{1}^{\bullet\bullet\bullet+}$ CH_2Cl_2 at 140 K. b) ESR spectra of 1 mM solution of triradical cation $\mathbf{1}^{\bullet\bullet\bullet+}$ in CH_2Cl_2 at 140 K at the half-field region.

Computational Details

Structures. The molecular geometries of the diradical (**1**¨) and triradical cation (**1**˙˙˙⁺) species have been optimized in their low-spin (LS, Singlet for **1**¨, Doublet for **1**˙˙˙⁺) and high-spin states (HS, Triplet for **1**¨, Quadruplet for **1**˙˙˙⁺), both for the *Z* and *E* isomers. All calculations have been performed at the UB3LYP/TZVP level using the D2 dispersion correction of Grimme[S1] as implemented in Gaussian 09.[S2] Dichloromethane solvent has been modelled using the PCM method.

Magnetic Properties. The magnetic exchange couplings (J_{AB}) have been evaluated on those structures at the same level of calculation. For **1**¨, we have calculated the energy of the triplet and Broken-Symmetry singlet and their energy difference has been directly used to compute J_1 using the isotropic Heisenberg Hamiltonian $\hat{H} = -2\sum_{A,B}^{N} J_{AB}\hat{S}_A\hat{S}_B$. In turn, for the triradical cation **1**˙˙˙⁺, we have calculated the energy of one quadruplet and three doublet states (one for each possible combination of two unpaired alpha and one beta electrons on the three magnetic units) and the resulting energy differences have been used to extract J_{1-3}.

Optical Properties. The absorption spectra have been calculated on the optimized geometries of the *Z* isomer of the neutral diradical and cationic-triradical species in their HS state. We have used the UB3LYP/TZP scheme as implemented in ADF 2013.[S3] Dichloromethane has been modelled using the PCM method.

Computational analysis of 1¨ and 1˙˙˙⁺:

Magnetic Properties. The ground state of **1**¨ is an open-shell singlet, with the two unpaired electrons localized in the PTM units (see Figure S15 and Table S1). They are coupled by an almost-negligible magnetic interaction (J_1, see Figure S16 and Table S2 and), whose strength indicates that no magnetic ordering would be observed even at low temperatures and that the system would effectively behave as paramagnet, with *ca.* 75% population of triplet states. This is consistent with the CV measurements and with the observation of the Δm_s = 2 transitions in the ESR spectrum.

In turn, the ground state of **1**˙˙˙⁺ is a doublet with three unpaired electrons localized in the TTF and PTM (x2) units (see Figure S17). The calculations indicate that the weak coupling between PTM units observed for **1**¨ is maintained, whereas moderately-strong antiferromagnetic (AFM) interactions appear between the oxidized TTF and each of the PTM moieties ($J_2 \approx J_3 \approx -60$ cm^{-1}).

Finally, it is worth mentioning that the anionic monoradical compound **1**˙⁻ has not been analyzed due to the well-known difficulty of describing mixed-valence states with DFT.[S4-S6]

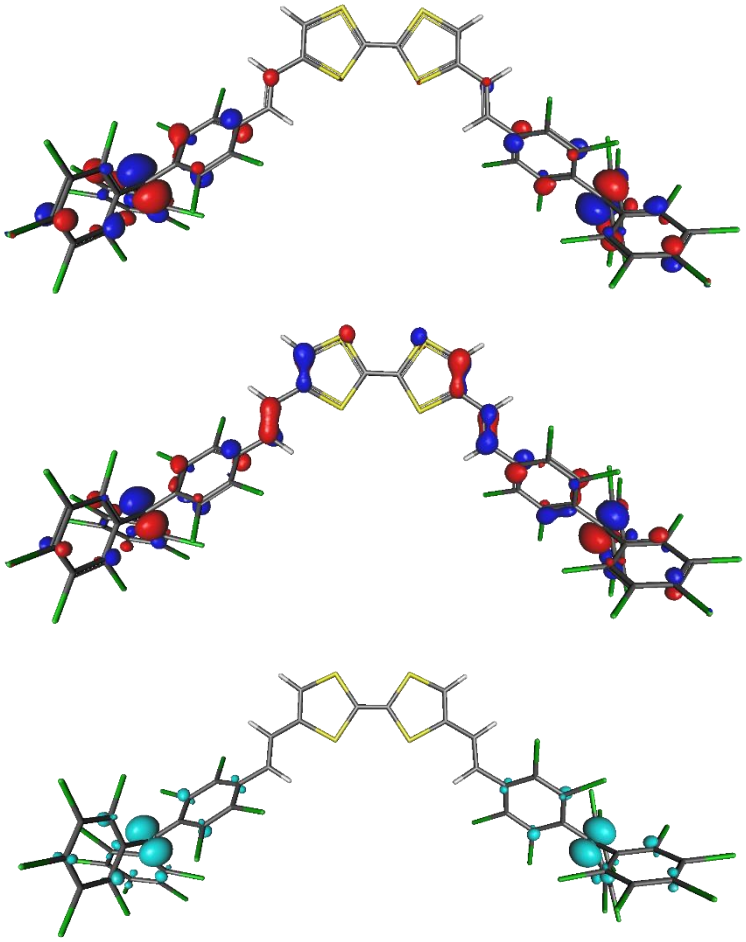

Figure S15. Singly-Occupied Molecular Orbital (SOMO) and spin density distribution obtained for the HS states of **1**·· (Isomer Z). SOMO isovalue = 0.04, Spin Density isovalue = 0.01.

Table S1. Spin density contained in the different constituents of **1**·· and **1**···+.

	1··		**1**···+	
Fragment	***Z***	***E***	***Z***	***E***
TTF	0.040	0.072	0.974	0.975
Vinylene Bridge	0.014	0.064	0.050	0.119
PTM #1	0.972	0.889	0.988	0.918
PTM #2	0.974	0.974	0.988	0.989
Total	2.000	2.000	3.000	3.000

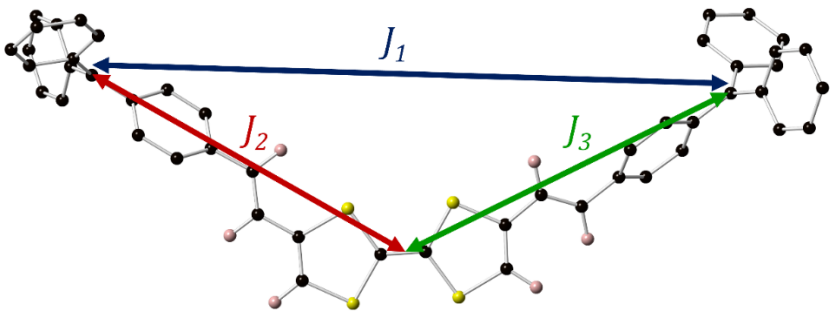

Figure S16. Representation of the magnetic interactions between the potential spin-carrying units of **1**. For clarity, the Cl atoms of the PTM moieties are not shown.

Table S2. Magnetic exchange couplings (J_{AB}, value in cm^{-1}) between unpaired electrons of the *Z* and *E* Isomers of **1**$^{\cdot\cdot}$ and **1**$^{\cdot\cdot\cdot+}$, labelled according to Figure S15.

1$^{\cdot\cdot}$		J_1	
Isomer-*Z*		<|0.05|	
Isomer-*E*		−0.6	
1$^{\cdot\cdot\cdot+}$	J_1	J_2	J_3
Isomer-*Z*	−0.7	−66.2	−62.9
Isomer-*E*	−0.5	−62.5	−59.3

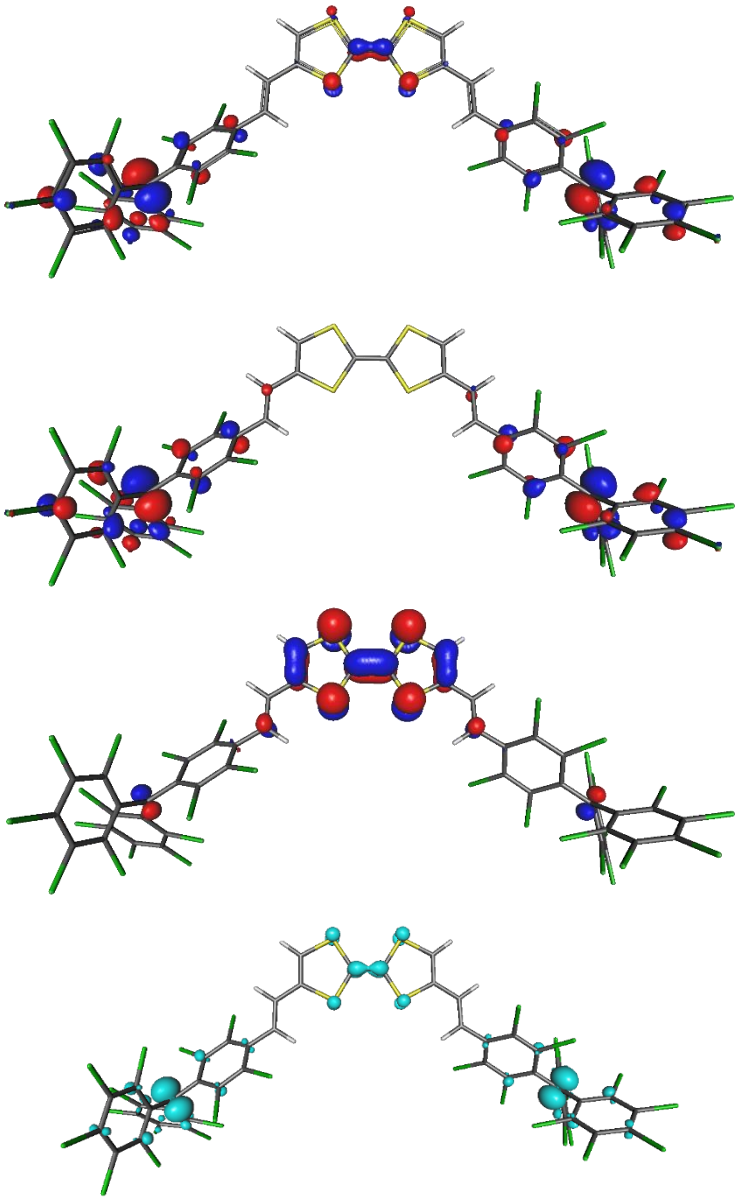

SOMO 1

SOMO 2

SOMO 3

Spin Density

Figure S17. Singly-Occupied Molecular Orbital (SOMO) and spin density distribution obtained for the HS states of **1**$^{\cdot\cdot\cdot+}$ (Isomer Z). SOMO isovalue = 0.04, Spin Density isovalue = 0.01.

Optical Properties. TDDFT calculations shed some light on the optical properties of the studied compounds. Even if the position of the calculated bands displays a shift toward larger energies - smaller wavelengths -, such analisys is useful to complement the rationalization of the spectra obtained experimentally. For compound **1**$^{\bullet\bullet}$, the calculations predict three main bands (Table S3). One in the near-IR (1401nm, oscillator stregth *fosc* = 0.1), corresponding to the charge transfer from the TTF HOMO to the PTM SUMO orbitals (see Figure S15). Since the two PTM units are not strictly equivalent, this transition apears as a double band (also 1338 nm, *fosc* = 0.03). This computed band corresponds to the experimental band observed at 900 nm, and the red-shift is associated to (*i*) the accuracy of the calculation, which implies larger shifts in the low-energy region, and (*ii*) to the simplicity of our inspection, which does not account for the effects derived from the fast *E-Z* isomerization. Two higher energy bands are also observed at 590 nm (*fosc* = 0.25) and 520 nm (*fosc* = 0.44). The first one corresponds to the transition from the TTF HOMO-1 to the PTM SUMO and the second one to the TTF HOMO to an unoccupied orbital delocalized over the Vinylene-PTM system.

Table S3. Main bands of the absorption spectra computed for (a) **1**$^{\bullet\bullet}$ and (b) **1**$^{\bullet\bullet\bullet+}$ in dichloromethane

1$^{\bullet\bullet}$	
Band	Type
520 nm, *fosc* = 0.44	TTF [HOMO] - Vinylene-PTM
590 nm, *fosc* = 0.25	TTF [HOMO-1] - PTM [SUMO]
1401 nm, *fosc* = 0.1	TTF [HOMO] - PTM [SUMO]
1$^{\bullet\bullet\bullet+}$	
Band	Type
510 nm, *fosc* = 0.65	TTF [SOMO] - Vinylene-PTM
687 nm, *fosc* = 0.45	TTF [HOMO] - PTM [SUMO]

Regarding **1**$^{\bullet\bullet\bullet+}$, our calculations yield two bright bands at 687 nm (*fosc* = 0.45) and 510 nm (fosc = 0.65) (see Table S3). The first one corresponds mainly (95%) to a transition from the TTF^{+} HOMO (HOMO-1 of the neutral TTF) to the PTM SUMO (see Figure S15). It is, thus, equivalent to the transition observed at 590 nm for the neutral compound. In turn, the second one is a mixture of several transitions, being dominant the one from the TTF^{+} SOMO (HOMO of the neutral TTF) to the Vinylene-PTM system, as observed for the neutral compound (band at 520 nm). As expected, the low-energy band observed for the neutral specie disappears upon TTF oxidation.

Structure. The molecular geometries of the diradical (**1**$^{\bullet\bullet}$) and triradical cation (**1**$^{\bullet\bullet\bullet+}$) species have been optimized in their low-spin (LS, Singlet for **1**$^{\bullet\bullet}$, Doublet for **1**$^{\bullet\bullet\bullet+}$) and high-spin states (HS, Triplet for **1**$^{\bullet\bullet}$, Quadruplet for **1**$^{\bullet\bullet\bullet+}$), both for the *Z* and *E* isomers and several conformations of the two vinylene bridges. Some of the values reported in Tables S4 and S5 have been used to extract the magnetic exchange couplings reported in Table S2.

Table S4. Computed energy differences (in kcal/mol) of the Z- and E- isomers of **1**$^{\bullet\bullet}$ in several conformations of the two vinylene bridges. The values are given with respect to the most stable one. The energy of the high-spin and low-spin states have been evaluated at each optimized structure.

Isomer	**Bridge 1**	**Bridge 2**	**Geometry**	**Spin State**	
				T	**S**
Z	cis	trans	S	2.90	2.90
Z	cis	trans	T	2.90	2.90
Z	trans	trans	S	0.02	0.02
Z	trans	trans	T	0.02	0.02
E	cis	trans	S	2.88	2.87
E	cis	trans	T	2.88	2.87
E	trans	trans	S	0.00	0.00
E	trans	trans	T	0.00	0.00

Table S5. Computed energy differences (in kcal/mol) of the Z- and E- isomers of $\mathbf{1}^{\bullet\cdot+}$ in several conformations of the two vinylene bridges. The values are given with respect to the most stable one. The energy of the high-spin and low-spin states have been evaluated at each optimized structure. For simplicity, we only include one possible doublet state, in which two alpha electrons are in the PTM units and one beta electron in the TTF.

Isomer	Bridge 1	Bridge 2	Geometry	Spin State	
				Q	D
Z	cis	trans	D	1.96	1.67
Z	cis	trans	Q	1.93	1.67
Z	trans	trans	D	0.37	0.00
Z	trans	trans	Q	0.33	0.01
E	cis	trans	D	2.00	1.74
E	cis	trans	Q	1.96	1.73
E	trans	trans	D	0.43	0.08
E	trans	trans	Q	0.39	0.09

References:

[S1] S. Grimme, *J. Comput. Chem.* **2006**, *27*, 1787-1799.

[S2] M. J. Frisch, G. W. Trucks, H. B. Schlegel, G. E. Scuseria, M. A. Robb, J. R. Cheeseman, G. Scalmani, V. Barone, B. Mennucci, G. A. Petersson, H. Nakatsuji, M. Caricato, X. Li, H. P. Hratchian, A. F. Izmaylov, J. Bloino, G. Zheng, J. L. Sonnenberg, M. Hada, M. Ehara, K. Toyota, R. Fukuda, J. Hasegawa, M. Ishida, T. Nakajima, Y. Honda, O. Kitao, H. Nakai, T. Vreven, J. A. Montgomery Jr., J. E. Peralta, F. Ogliaro, M. Bearpark, J. J. Heyd, E. Brothers, K. N. Kudin, V. N. Staroverov, R. Kobayashi, J. Normand, K. Raghavachari, A. Rendell, J. C. Burant, S. S. Iyengar, J. Tomasi, M. Cossi, N. Rega, J. M. Millam, M. Klene, J. E. Knox, J. B. Cross, V. Bakken, C. Adamo, J. Jaramillo, R. Gomperts, R. E. Stratmann, O. Yazyev, A. J. Austin, R. Cammi, C. Pomelli, J. W. Ochterski, R. L. Martin, K. Morokuma, V. G. Zakrzewski, G. A. Voth, P. Salvador, J. J. Dannenberg, S. Dapprich, A. D. Daniels, Ö. Farkas, J. B. Foresman, J. V. Ortiz, J. Cioslowski and D. J. Fox, 2009.

[S3] ADF2013, SCM, Theoretical Chemistry, Vrije Universiteit, Amsterdam, The Netherlands.

[S4] M. Kaupp, M. Renz, M. Parthey, M. Stolte, F. Wurthner and C. Lambert, *Phys. Chem. Chem. Phys.* **2011**, *13*, 16973-16986.

[S5] V. Lloveras, J. Vidal-Gancedo, T. M. Figueira-Duarte, J.-F. Nierengarten, J. J. Novoa, F. Mota, N. Ventosa, C. Rovira and J. Veciana, *J. Am. Chem. Soc.* **2011**, *133*, 5818-5833.

[S6] M. Fumanal, F. Mota, J. J. Novoa and J. Ribas-Arino, *J. Am. Chem. Soc.* **2015**, *137*, 12843-12855.